Flange Local Buckling Resistance and Local–Global Buckling Interaction in Slender-Flange Welded I-Section Beams

WAJAHAT LATIF and DONALD W. WHITE

ABSTRACT

AISC *Specification* Chapter F characterizes the flange local buckling (FLB) strength of I-section members having a slender compression flange as the theoretical elastic plate local buckling resistance, ignoring beneficial local post-buckling strength. Previous research has shown that this results in highly conservative strength predictions for slender-flange members. Additionally, potential interaction between local and global lateral-torsional buckling modes is not considered in the AISC *Specification*. These aspects can be important in applications involving the use of slender-flange members. This paper investigates a number of potential methodologies to account for local post-buckling strength as well as local–global buckling interaction in beams having slender flanges. A parametric finite element analysis (FEA) study is conducted considering a range of I-section members. The strength predictions from the proposed methodologies and the AISC *Specification* are evaluated against the FEA results as well as against a database of measured strengths from previous experimental tests of I-section beams governed by FLB. Recommendations are provided focusing on simplicity of the calculations and the efficacy of their predictions.

Keywords: flange local buckling, lateral-torsional buckling, local–global buckling interaction, plate effective width.

INTRODUCTION

The AISC *Specification for Structural Steel Buildings* (AISC, 2016), hereafter referred to as the AISC *Specification*, idealizes the strength of slender-flange I-section beams as the theoretical elastic plate local bucking resistance. This handling of slender-flange members fails to recognize the flange local post-buckling reserve strength and tends to give very conservative predictions as the compression flange becomes more slender. This conservatism is evident from experimental tests documented by White and Jung (2008) and White and Kim (2008). In addition, analytical studies by Seif (2010), Seif and Schafer (2010), Toğay (2018), Toğay and White (2018), Gerard (2020), and Latif (2020) reveal the presence of significant local post-buckling capacity of slender-flange, I-section members loaded in flexure.

One application of slender flanges is in metal building design where it is common to use constant-width flanges while stepping the flange thicknesses, tapering the web depths, and/or stepping the web thicknesses to achieve design economy. In these types of structures, slender compression flanges can be economical in areas of low bending moment demand. Moreover, as the use of higher strength steels becomes more common, a greater number of cases will classify as having slender flanges since the noncompact-flange limit, λ_{rf}, becomes smaller. These aspects of design practice provide the impetus for development of a more accurate FLB strength characterization recognizing the local post-buckling strength of slender flanges.

As the compression flange becomes more slender, the flange local buckling response may have a significant influence on the global lateral-torsional buckling (LTB) strength of the member, due to local–global buckling interaction. The AISC *Specification* does not address this interaction. It is assumed implicitly that the flange local buckling (FLB) predictions for slender flanges are sufficiently conservative such that local–global strength interaction can be neglected. With the development of an improved procedure for predicting the FLB strength of slender-flange members accounting for post-buckling resistance, it may be important to address potential local–global interaction. Early experimental research by Cherry (1960) indicated the presence of significant local–global interaction in thin flange members. More recent analytical studies by Gerard (2020) and Latif (2020) have also shown this behavior.

This paper considers several methodologies for improved prediction of the flexural resistance of slender-flange I-section members accounting for local post-buckling strength and local–global buckling interaction. The procedures are evaluated using nonlinear shell finite element analysis as well as by comparison to previous experimental results.

Wajahat Latif, Research Affiliate, School of Civil and Environmental Engineering, Georgia Institute of Technology, Atlanta, Ga. Email: wajahatlatif@hotmail.com

Donald W. White, Professor, School of Civil and Environmental Engineering, Georgia Institute of Technology, Atlanta, Ga. Email: dwhite@ce.gatech.edu (corresponding)

Paper No. 2021-05

METHODOLOGIES STUDIED

This section outlines five methodologies studied to characterize the post-buckling strength and local–global buckling interaction in slender-flange members. Representative FLB strength curves from these methodologies, and from the AISC *Specification*, are presented in Figure 1. Figures 2 and 3 outline the FLB and LTB calculations, respectively, for each approach via flowcharts employing a unified format to simplify the process of understanding their logical flow. The reader should note that the AISC *Specification* approach in these figures is shown in the form employed within the AISC/MBMA Design Guide 25 (White et al., 2021), which combines AISC *Specification* Section F4 and F5 provisions into one set of calculations. For instance, using the combined Section F4 and F5 provisions, R_{pg} is taken equal to 1.0 for compact- and noncompact-web members. The reader is referred to AISC *Specification* Sections F4 and F5 for the equations corresponding to R_{pg} and R_{pc}.

Effective Width Methods

The unified effective width method, developed by Peköz (1986), recognizes that slender plate elements are not able to develop full yielding on their gross cross section at their ultimate strength. These elements undergo local buckling, resulting in a loss of stiffness and redistribution of stresses. A plate element subjected to a given member critical compressive stress, F_{cr}, is effective for only a portion of its full width. This effective width is given by the AISC *Specification* Equations E7-2 and E7-3, which may be written as the single equation

$$b_e = \min\left[b_{fc}\left(1-0.22\sqrt{\frac{F_{el}}{F_{cr}}}\right)\sqrt{\frac{F_{el}}{F_{cr}}}, b_{fc}\right] \tag{1a}$$

This equation is commonly referred to as Winter's (1970) curve. In the application of Equation 1a, the flange elastic local buckling stress may be written as

$$F_{el} = \frac{0.9Ek_c}{\lambda_f^2} \tag{1b}$$

in which k_c is a flange local buckling coefficient and λ_f is the flange slenderness $b_f/2t_f$. The calculation of the member strength using the compression flange effective width obtained from Equation 1a inherently recognizes the post-buckling capacity of slender flange elements. Four approaches are considered in this research that utilize Winter's curve to define member FLB strengths. These approaches are denoted by the abbreviations EW, EW_{Fy}, EW-LG, and REW_{Fy}, where EW, REW, and LG stand for "effective width," "refined effective width," and "local–global interaction," respectively.

In these approaches, the noncompact-flange limit is given by $\lambda_{rf.new} = 0.64\sqrt{k_c E/F_y}$ as recommended by Schafer et al. (2020), instead of AISC *Specification* $\lambda_{rf.AISC} = 0.95\sqrt{k_c E/F_L}$ (with F_L taken equal to $0.7F_y$ for doubly symmetric sections). The limit $\lambda_{rf.AISC}$ is tied to the anchor point at $0.7M_{yc}$ on the AISC *Specification* theoretical elastic FLB strength curve. Conversely, the limit $\lambda_{rf.new}$ is tied to a point on Winter's curve, where the effective width of the compression flange reaches the full gross width, b_f. Therefore, $M_n = R_{pg}M_{yc}$ at $\lambda_f = \lambda_{rf.new}$, where $R_{pg} = 1$ for compact- and noncompact-web members. For $\lambda_f > \lambda_{rf.new}$, the strengths are defined by using Equation 1a for the compression flange effective width.

Based on recent research, several improvements to the LTB strength and noncompact-web slenderness limit, λ_{rw}, characterizations are incorporated in all the effective width methodologies considered in this paper:

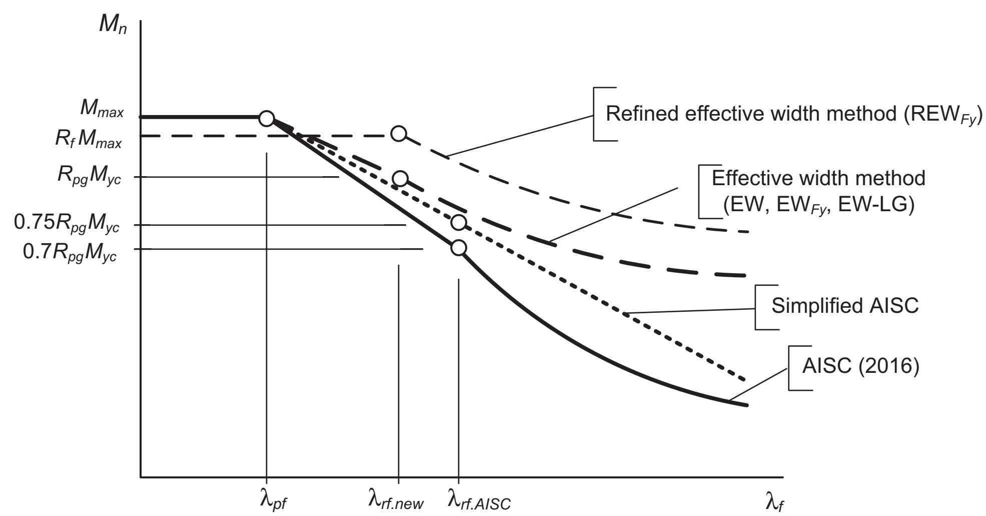

Fig. 1. Illustration of FLB curves based on the approaches studied.

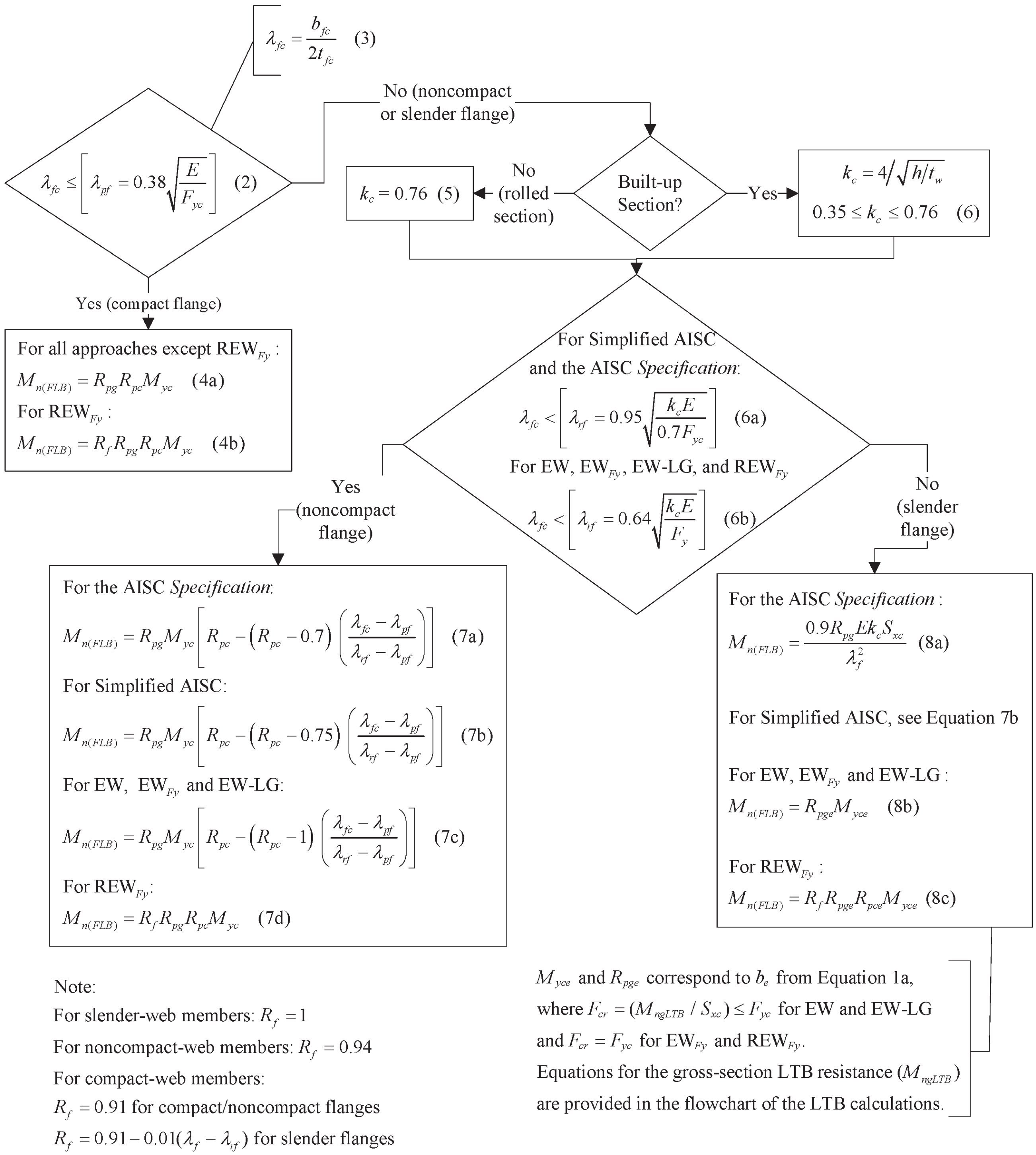

Fig. 2. FLB calculations for I-section beams for all methodologies.

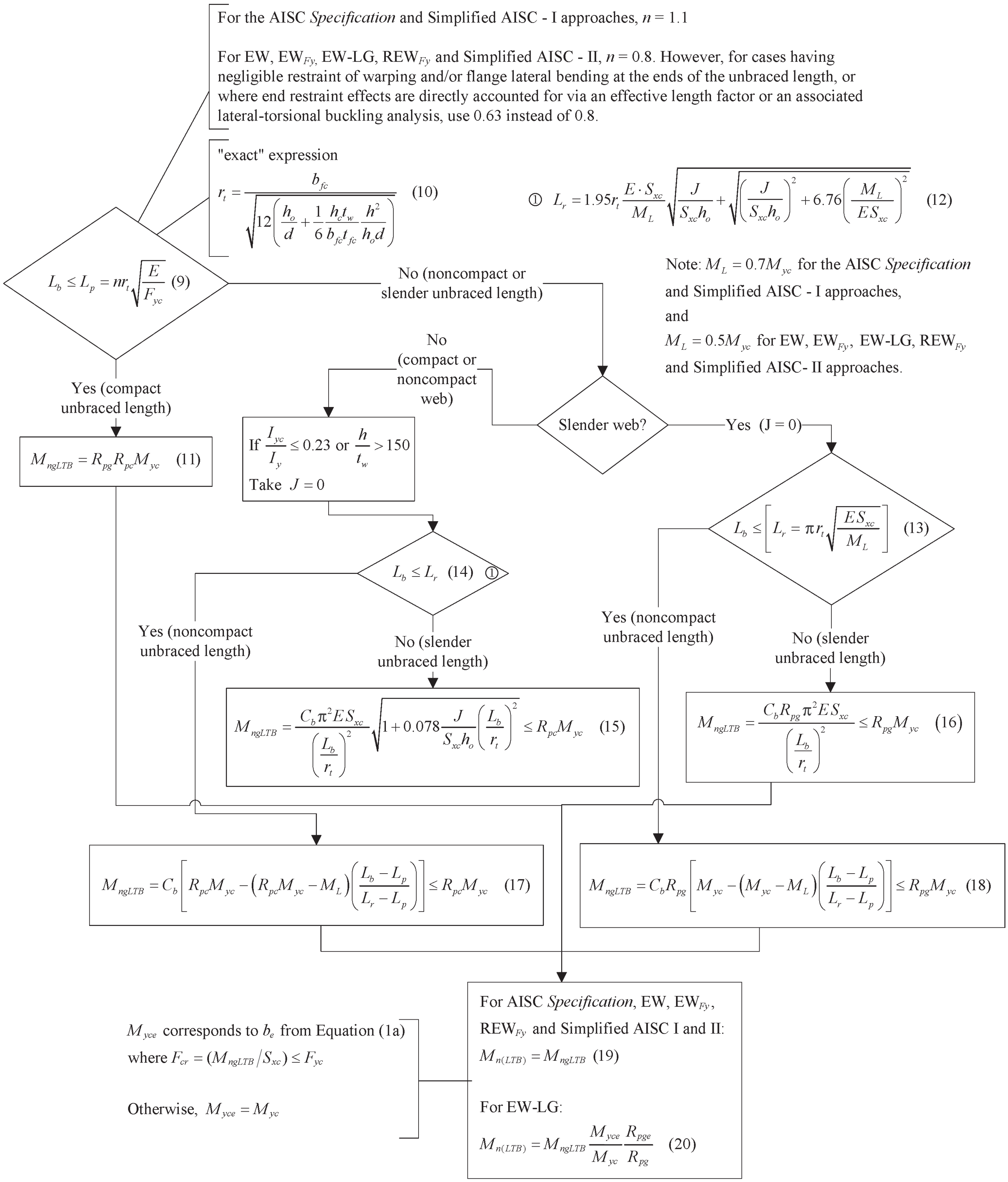

Fig. 3. LTB calculations for I-section beams for all methodologies.

a. Consistent with the recommendations proposed in Subramanian et al. (2018), the compact unbraced length limit, L_p, is taken as $0.63r_t\sqrt{E/F_y}$. Subramanian et al. recommend this limit for cases having negligible warping and flange lateral bending restraint at the ends of unbraced length and for cases where end restraint effects are directly accounted for in the resistance calculations.

b. The maximum moment level above which the characterization of the strength by theoretical elastic LTB is no longer sufficient, due to residual stresses, geometric imperfections, and second-order flange lateral bending effects, is taken as $M_L = 0.5M_{yc}$ as recommended by Subramanian et al. (2018) rather than the value used in the AISC *Specification* ($0.7F_yS_{xc}$ for doubly symmetric sections).

c. Based on the recommendations by Subramanian and White (2017b, 2017d), the noncompact-web slenderness limit is taken as $\lambda_{rw} = c_{rw}\sqrt{E/F_y}$, where $c_{rw} = \max\left[\min(5.7,\ 3.1+5/a_w), 4.6\right]$. This modification influences both the LTB and the FLB strength estimates.

The different effective width approaches may be distinguished as follows.

EW Approach

In the EW approach, the FLB strength of slender-flange members is characterized based on the effective section properties obtained from Equation 1a using the global buckling stress $F_{cr} = (M_{ngLTB}/S_{xc} \le F_{yc})$, where M_{ngLTB} is the global LTB strength. The LTB strength calculations in this procedure are based on the gross cross section.

EW_{Fy} Approach

This approach is similar to the EW approach except that the effective width of the slender flange is calculated at the yield strength (i.e., F_{cr} is taken equal to F_y in Equation 1a).

EW-LG Approach

This approach addresses the FLB strength calculations in a similar manner to the EW approach. However, in addition, the global LTB strength is calculated using the effective section properties to account for a loss in member global buckling capacity resulting from local buckling. That is, an effort is made to directly characterize and account for local–global buckling interaction. The effective width is calculated based on $F_{cr} = (M_{ngLTB}/S_{xc} \le F_{yc})$, where M_{ngLTB} is the global LTB strength based on gross section properties.

Refined Effective Width Method (REW_{Fy})

This procedure is a form of the effective width approach, modified such that the Winter's curve characterizing the strength of slender flanges starts at a plateau resistance, M_{max}, larger than M_{yc} for members with noncompact or compact webs, as illustrated in Figure 1. The critical stress, F_{cr}, in Equation 1a is taken equal to the yield stress, F_y. Furthermore, a curve-fitting variable, R_f, is introduced in the FLB strength curve based on FEA results discussed later. The LTB strength calculations are based on gross cross-section properties.

Simplified AISC Method

A simplified procedure is proposed that uses a straightforward modification of the AISC *Specification* FLB strength curve to provide an accurate to conservative characterization of the significant local post-buckling resistance of I-section member compression flanges with $b_f/2t_f$ values approaching or exceeding the noncompact slenderness limit, $\lambda_{rf.AISC} = 0.95\sqrt{k_c E/F_L}$, where F_L is taken equal to $0.7F_{yc}$. In this procedure, the ordinate of the flange local buckling resistance is increased from $0.7M_{yc}$ to $0.75M_{yc}$ at $\lambda_{rf.AISC}$. Furthermore, the noncompact-flange local buckling equation is extended to members with slender compression flanges as a streamlined conservative characterization of the flange post-local buckling strength for these member types. This approach is a simplification of an approach recommended by Toğay (2018) and Toğay and White (2018), where the second anchor point on the noncompact-flange FLB curve, at the noncompact-flange limit, was defined as the point on Winter's curve at $\lambda_{rf.AISC.}$

Using this procedure for the FLB assessment, the following two calculations are considered depending on the handling of the LTB strength and the noncompact-web slenderness limit.

Simplified AISC–I

In this procedure, the LTB strength and the noncompact-web slenderness limit calculations are employed as defined in the AISC *Specification*.

Simplified AISC–II

In this procedure, the recommended LTB strength and noncompact-web slenderness limit calculations outlined in Section 2.1, from Subramanian et al. (2018) and Subramanian and White (2017b, 2017d), are employed.

Table 1. Test Members for FEA Studies Focused on Evaluating Flange Post-Buckling Resistance ($b_f = 9$ in., $h = 28$ in., $L_b = 25$ in., $F_Y = 55$ ksi)			
Test Category	**Test Name**	$b_f/2t_f$	h/t_w
Slender-web members	SW-7	7	149
	SW-9	9	149
	SW-11	11	149
	SW-13	13	149
	SW-15	15	149
	SW-18	18	149
Noncompact-web members	NCW-7	7	93.3
	NCW-9	9	93.3
	NCW-11	11	93.3
	NCW-13	13	93.3
	NCW-15	15	93.3
	NCW-18	18	93.3
Compact-web members	CW-7	7	70.0
	CW-9	9	70.0
	CW-11	11	70.0
	CW-13	13	70.0
	CW-15	15	70.0
	CW-18	18	70.0

FEA STUDIES

The FEA studies in this research focus on doubly symmetric I-section members. All the test members have homogenous material properties and a single unbraced length, braced against out-of-plane lateral deflection and twisting at the member ends. Multipoint constraints are implemented that enforce Vlasov kinematics at the member ends (plane sections remain plane except for warping of the flanges) as described by Kim (2010). The study is divided into two main investigations as detailed in the following sections.

Characterization of the FLB Limit State

The first FEA study is designed to evaluate the FLB resistances in the absence of significant LTB slenderness effects. The unbraced length of these members is held constant at ($L_b = 25$ in.) $< L_p$ to ensure plateau strength LTB conditions. The calculated L_p values for the sections studied range from 26.8 to 34.8 in. The flange and web thicknesses are varied to study a range of flange slenderness values for compact-web, noncompact-web, and slender-web sections. All the members have an assumed yield strength of 60 ksi (representative of typical measured yield strengths for Grade 55 steels) and are subjected to uniform moment. Table 1 outlines the members considered. The test names are selected to reflect the web and flange slenderness values of the members. SW, NCW, and CW denote "slender," "noncompact," and "compact webs," respectively, while the number at the end of the name is the flange slenderness value, $b_f/2t_f$.

Investigation of Local–Global Buckling Interaction

The following additional FEA test simulations are conducted to evaluate member cross sections and lengths potentially most susceptible to local–global buckling interaction. The targeted test members are classified into six cases as outlined in Table 2.

A flange slenderness of $b_f/2t_f = 18$ is selected for all the members in the local–global buckling interaction study. This is the upper limit of allowable flange slenderness recommended by AISC Design Guide 25 (White et al., 2021) and represents a relatively thin flange case. The post-buckling deformations of these flanges are expected to have significant potential impact on the global buckling strength. The slender-web sections studied have relatively deep webs compared to the compact-web sections, which have relatively shallow webs. The shallower webs are selected to evaluate situations where the strength may be more sensitive to the FLB behavior. This is because the elastic properties of these sections, such as the moment of inertia, have a

Table 2. Test Cases for Study of Potential Local–Global Buckling Interaction (b_f = 9 in. and $b_f/2t_f$ = 18 in.)				
Case	Description	Test Names	h/t_w	h
1	Slender flange–slender web, uniform moment, F_y = 60 ksi	UM-Lb#-SF-SW-60	149	28
2	Slender flange–slender web, uniform moment, F_y = 100 ksi	UM-Lb#-SF-SW-100	149	28
3	Slender flange–compact web, uniform moment F_y = 60 ksi	UM-Lb#-SF-CW-60	36.0	9
4	Slender flange–compact web, uniform moment F_y = 100 ksi	UM-Lb#-SF-CW-100	36.0	9
5	Slender flange–slender web, moment gradient, F_y = 60 ksi	MG-Lb#-SF-SW-60	149	28
6	Slender flange–slender web, moment gradient, F_y = 100 ksi	MG-Lb#-SF-SW-100	149	28

smaller contribution from the web. A number of beams are subjected to a linearly varying moment (maximum moment at one end of the unbraced length and zero moment at the other end) in this study, in addition to specimens subjected to uniform bending.

The unbraced lengths for each section type are varied to investigate local–global buckling interaction. The notation for the test names is selected to uniquely define each member. For example, test member UM-LB85-SF-SW-60 indicates a member subjected to uniform moment with an unbraced length of 85 in, slender flanges, a slender web and F_y = 60 ksi. The notations MG and CW appearing in the test names in Table 2 stand for "moment gradient" and "compact web," respectively.

FINITE ELEMENT MODELING PARAMETERS

Element Type and FEA Discretization

The webs and flanges of the members are modeled using the S4R element in ABAQUS (Simulia, 2013), which is a four-node, quadrilateral, large-strain shell element. The members are evaluated using full, nonlinear finite element analysis, including material and geometric nonlinearity. The mesh density corresponds to 12 elements across the flange width and 30 elements through the web depth for the 28-in. deep web members. For the 9-in. deep web members studied, 12 elements are employed through the web depth. These relatively dense meshes perform well in terms of convergence of the finite element solution and are selected based on the mesh discretization studies by Subramanian (2015). The number of elements along the length is calculated such that the aspect ratio of each element is approximately 1.0 within the web.

Material Properties

The test members are modeled using a J2 plasticity model with isotropic hardening. All test sections have homogenous material properties corresponding to either F_y = 60 ksi or F_y = 100 ksi, depending on the test case being studied. The modulus of elasticity, E, is taken as 29,500 ksi, which represents a common mean value for structural steels. For the Grade 60 steels, intended to be representative of the actual yield strength in typical metal building frame members fabricated with Grade 55 steels, the post-elastic stress-strain response is modeled with a tangent stiffness of $E/1000$ up to a strain-hardening strain value of 10 times the yield strain, ε_y. The strain-hardening modulus is idealized as $E/50$ after this point. This is a common representation of the stress-strain response of ordinary structural steels (ASCE, 1971) and is adequate for the test simulations under consideration since the strain levels observed exceed the strain hardening strain by a minor amount and only within localized regions in these studies. For the Grade 100 steels, F_y is modeled directly as 100 ksi, and a constant post-elastic tangent stiffness of $E/1000$ is employed without any characterization of strain hardening. This provides a representation of the stress-strain response for some of these types of steels, such as the plates employed in the girder tests by Fahnestock and Sause (1998). Some high-strength steels do not exhibit a sharp yield response. This potential attribute is not addressed in this research.

Residual Stresses

The best-fit Prawel residual stress pattern used previously by Kim (2010) and Subramanian (2015) has been adopted for these studies. The residual stress values are halved based on the recommendations for LTB tests by Subramanian and White (2017a, 2017b, 2017c) to correlate with the mean results from experimental tests. Additionally, the web residual stresses are taken equal to zero. This is a reasonable approximation for the slender web h/t_w values studied since the slender webs would buckle prior to reaching the base value for the web compressive residual stresses defined in the best-fit Prawel pattern. For the members with compact webs, the web can sustain these compressive stresses; however, the residual stresses in the web have a minor impact on the member response in these cases. The residual stress pattern employed for all the studies is illustrated in the left diagram in Figure 4. In addition, the test cases in Table 1 are simulated using the full best-fit Prawel residual stress pattern, including residual stresses in the web. The full residual stress pattern is shown in the right-hand diagram in Figure 4.

Geometric Imperfections

Three types of geometric imperfections—namely, flange tilt, web out-of-flatness, and flange sweep—are considered. The flange tilt and web out-of-flatness patterns are obtained by executing an elastic eigenvalue buckling analysis of the test member subjected to uniform axial compressive stress, and in which the web-flange juncture locations are continuously constrained against lateral displacement.

The flange tilt in the buckling mode obtained for the flanges is scaled to one-half of the tolerance recommended in CEN (2006) and the out-of-flatness in the buckling mode for the web is scaled to one-half of the tolerance value in the *Metal Building Systems Manual* (MBMA, 2012). Recent research (Subramanian and White, 2017a) has shown that geometric imperfections of one-half typical specified tolerance values provide close correlation with the mean predictions from experimental LTB results. These one-half tolerance values are shown in Figure 5.

A flange sweep equal to approximately one-half of the value noted in AWS (2020) is applied at the web-compression flange juncture as shown in Figure 6. The tension flange is held straight when generating this imperfection.

In addition to these recommended one-half tolerance values, the test cases in Table 1 are also simulated with the full geometric imperfections. It should be noted that the full flange tilt imperfection from CEN (2006) is approximately 40% of the corresponding more restrictive value of the flange tilt tolerances from MBMA (2012), and the full flange sweep tolerance from AWS (2020) is approximately one-half the corresponding general member flange sweep tolerance in MBMA (2012).

RESULTS AND DISCUSSION

Characterization of the FLB Limit State

Figures 7 through 9 compare the FEA results for the test cases outlined in Table 1 with the strength predictions from the methodologies listed earlier for the slender-,

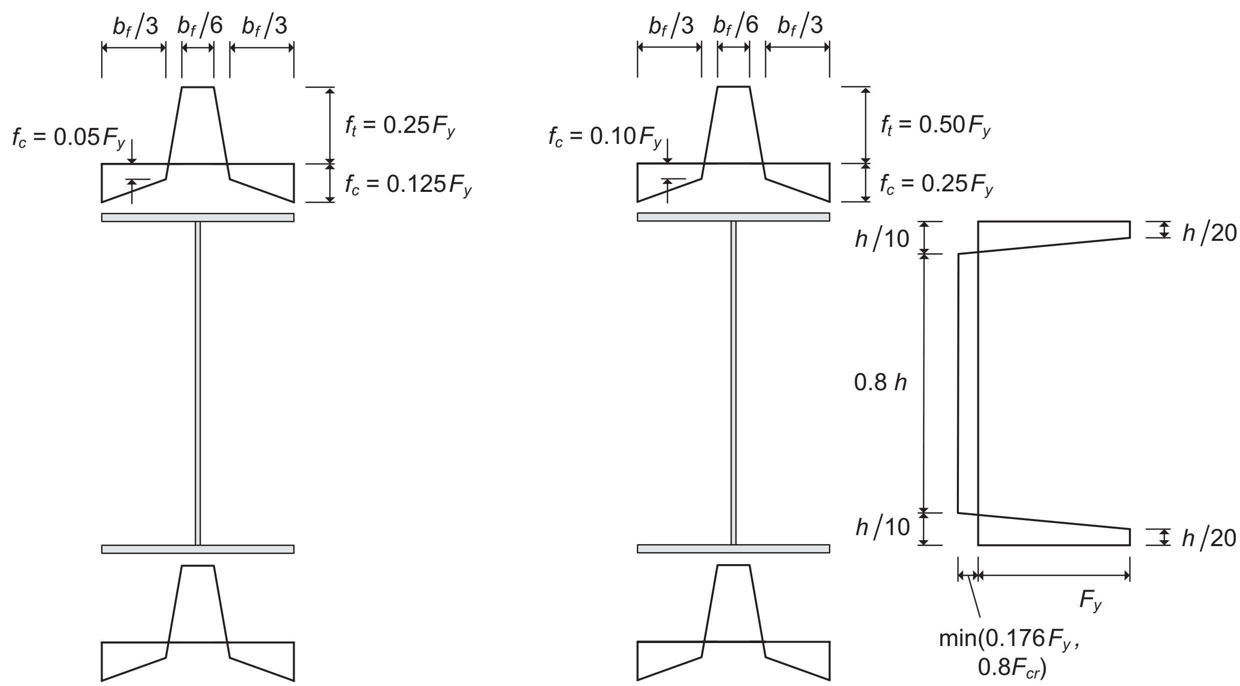

Fig. 4. Half residual stress pattern (left) and full residual stress pattern, including web stresses (right) employed in finite element analysis simulation studies.

noncompact-, and compact-web test members, respectively. In these plots, FEA(H) denotes FEA simulation results using the half residual stress and half geometric imperfection patterns, while FEA(F) denotes results using the full residual stress and full geometric imperfection patterns. Because the strength of all these members is governed by FLB, the EW and EW-LG procedures give the same predictions. Also, the critical stress, F_{cr}, is equal to F_y for these noncompact- and compact-web members, while it is very close to F_y for the slender-web members (M_{ngLTB} is reduced slightly below the yield moment by the strength reduction factor R_{pg} for the slender-web sections). For this reason, the predictions by the EW_{Fy} method are either equal to, or very close to, the EW and EW-LG predictions (i.e., the curves are indistinguishable even in cases where there are small differences). Therefore, the strength predictions by the EW, EW-LG, and EW_{Fy} methods are simply referred as EW in the plots. Similarly, the simplified AISC-I and AISC-II calculations are shown by a single strength curve, labeled as Simplified AISC, since these procedures only differ in their treatment of the LTB strength calculations (which do not govern for these test cases).

It is evident from these plots that the AISC *Specification* procedure gives highly conservative predictions compared to both the FEA(H) and FEA(F) results as the flange slenderness increases. This conservatism at high flange slenderness values is reduced by the use of the Simplified AISC curve. The EW curve consistently gives good correlation with the FEA(F) results for all three plots at the larger flange slenderness values, while the REW_{Fy} curve gives slightly conservative to accurate predictions for FEA(H) tests but significantly overestimates the FEA(F) strengths for the noncompact- and compact-web cases. However, for the noncompact- and compact-web cases, the EW curve suggests a rapid decrease in the strength when the flange slenderness is varied between the compact and noncompact limits. This rapid drop in the predicted capacity is an attribute of the EW approach and is not representative of physical or FEA simulation test data. Conversely, for slender-web members, the FLB strength curve does not have any noncompact-flange region in the EW calculations. That is, in the EW procedures, the start of the FLB strength reduction on Winter's curve corresponds to the plateau strength, $R_{pg}M_{yc}$. The REW_{Fy} procedure uses a curve fitting variable, R_f, to achieve more accurate predictions of the FEA(H) simulation results for the compact- and noncompact-web members. The difference between the strength predictions by the FEA(F) and FEA(H) solutions provides an indication of

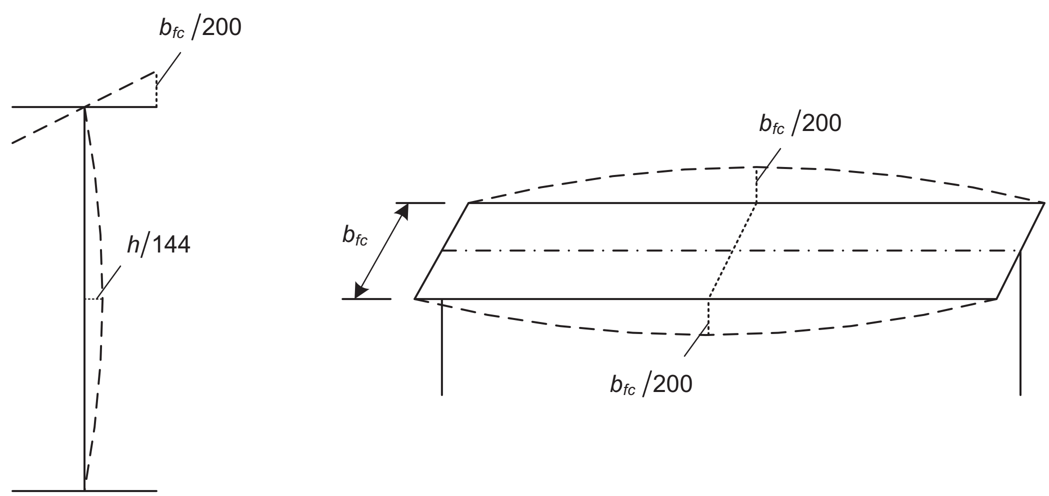

Fig. 5. Recommended one-half tolerance web out-of-flatness and flange tilt imperfections.

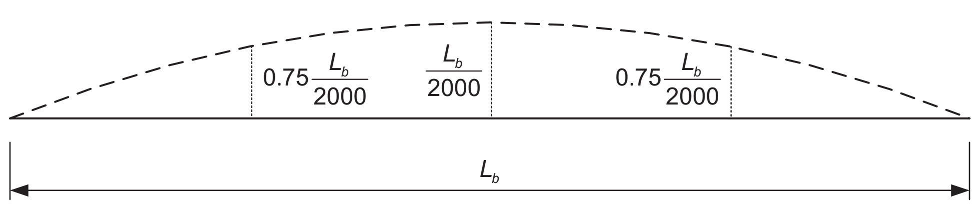

Fig. 6. Recommended one-half tolerance flange sweep imperfection.

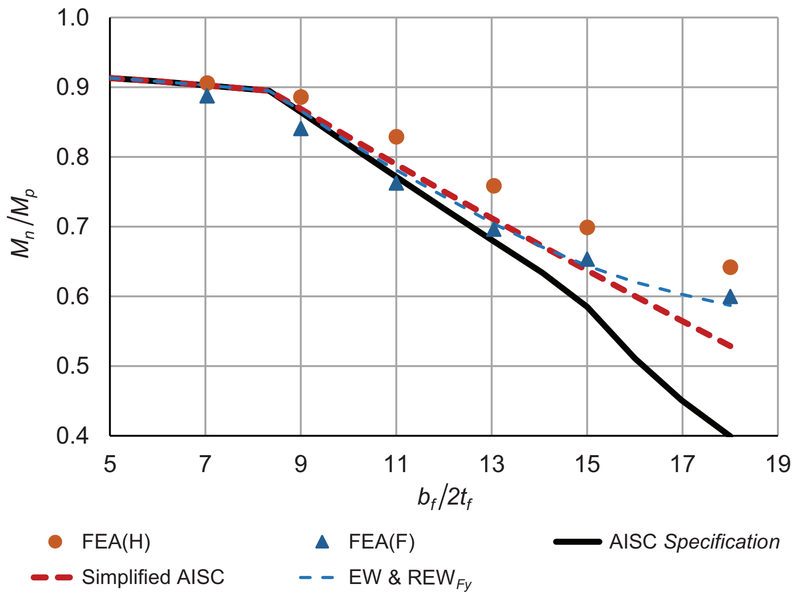

Fig. 7. Comparison of strength predictions by FEA simulations and different methodologies versus flange slenderness for slender-web members.

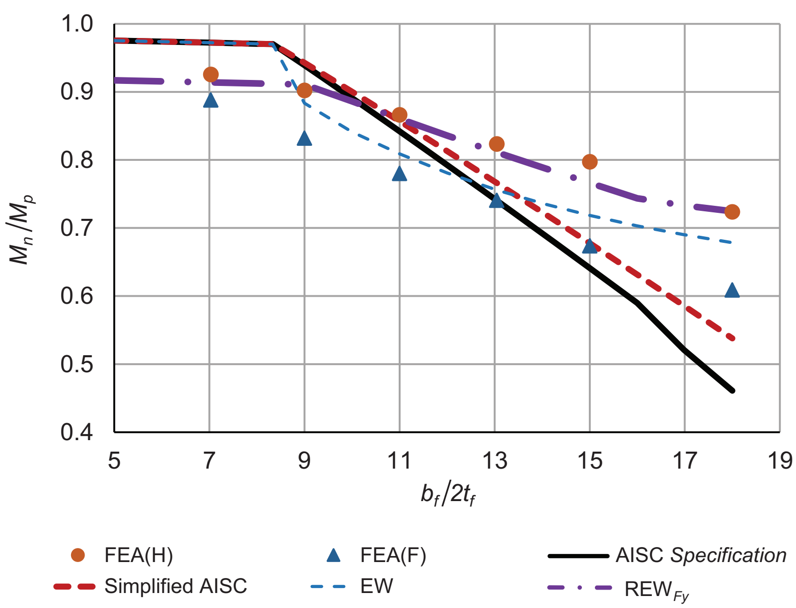

Fig. 8. Comparison of strength predictions by FEA simulations and different methodologies versus flange slenderness for noncompact-web members.

the sensitivity to variations in the residual stresses and geometric imperfections that might be experienced in physical members.

It is noted that the FEA results do not attain the plateau strength, $R_{pc}M_{yc,}$ for the compact-flange members corresponding to the smaller $b_f/2t_f$ values in Figures 8 and 9. However, the available experimental data (White and Jung, 2008; White and Kim, 2008), summarized earlier, indicates that the FLB plateau strengths are indeed achieved at the defined compact-flange limits.

Investigation of Local–Global Buckling Interaction

The results for test cases 1 to 6 (Table 2) are shown in Figures 10 through 15. These are plotted as the professional bias factor, M_{FEA}/M_n, where M_{FEA} is the strength determined from the FEA simulation and M_n corresponds to the strength predicted by any of the six procedures being evaluated. The solid markers along the respective curves denote the instances where the LTB equations govern, while the hollow markers indicate the cases where the FLB equations govern. Table 3 provides overall summary statistics for the professional bias factor, M_{FEA}/M_n, of all the methods for these six test cases, all having $b_f/2t_f = 18$.

The AISC *Specification* procedure tends to give the greatest conservatism and the largest dispersion of the predictions of all the methods (mean M_{FEA}/M_n of 2.56 and COV = 0.31 for all the conducted tests). The Simplified AISC-I approach mitigates this conservatism for both 60 ksi and 100 ksi members. However, as illustrated by Figures 10, 12, and 13, both the AISC *Specification* and Simplified AISC-I procedures exhibit M_{FEA}/M_n values less than 1.0 in certain tests. These tests correspond to members where the strength predictions are governed by the AISC *Specification* LTB calculations. These predictions are improved by using the recommended LTB and web noncompact limit, λ_{rw}, calculations in the Simplified AISC-II method.

All the other methods aim to capture the post-buckling strength of the slender compression flange by using an effective width approach. The EW procedure performs well for the cases with $F_y = 60$ ksi; however, these predictions tend to be unconservative for 100-ksi members (mean $M_{FEA}/M_n = 0.97$ and minimum $M_{FEA}/M_n = 0.84$). This is due to a lack of accounting for local–global interaction because the LTB calculations are based on the gross cross-section properties. In contrast, the EW-LG procedure provides conservative predictions on average (mean $M_{FEA}/M_n = 1.17$ for all of the tests) and has the smallest dispersion of all the methods considering all of the tests (maximum $M_{FEA}/M_n = 1.33$, minimum $M_{FEA}/M_n = 0.94$, and a COV of 0.07). The differences between the EW and EW-LG predictions shows that the 100-ksi members studied are more susceptible to local-global buckling interaction than the 60-ksi members.

The strength predictions by the EW_{Fy} and REW_{Fy} procedures overlap for all the slender-web members, where $R_f = 1.0$, and for all the tests governed by LTB because the LTB strength calculations are the same for both of these methods. Similar to the EW procedure, the EW_{Fy} and REW_{Fy} methods perform well for members with $F_y = 60$ ksi; however, the predictions tend to be unconservative for 100-ksi members at certain unbraced lengths due

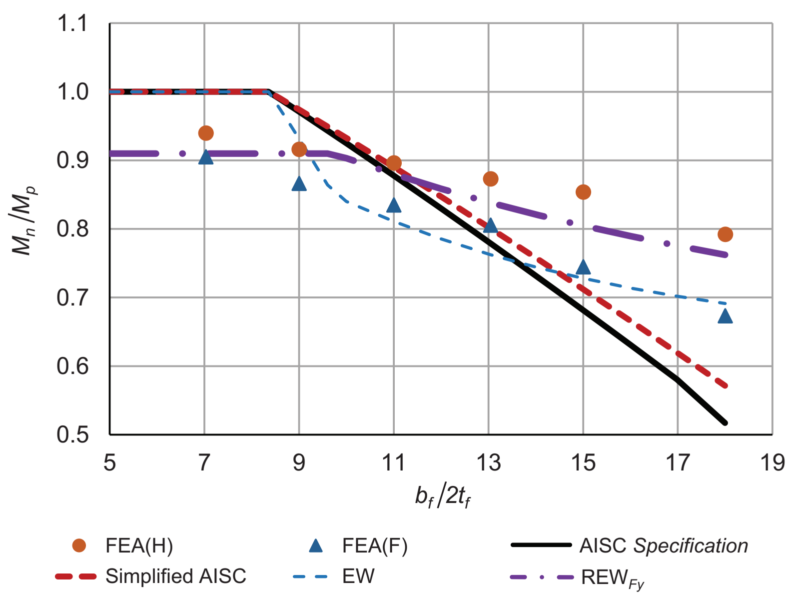

Fig. 9. Comparison of strength predictions by FEA simulations and different methodologies with flange slenderness for compact-web members.

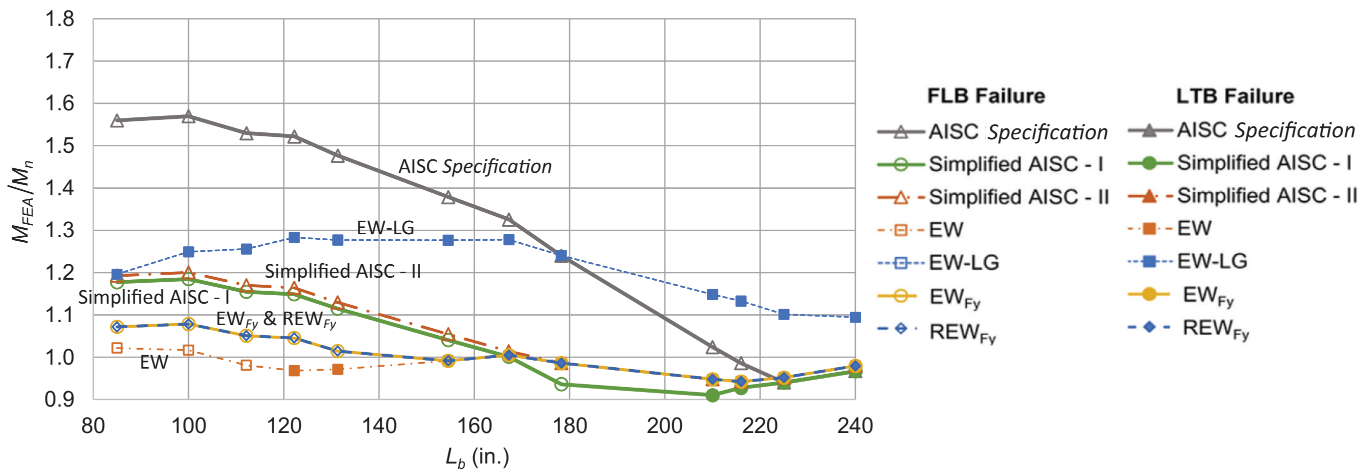

Fig. 10. Comparison of M_{FEA}/M_n *for case 1 members (slender-flange–slender-web members subjected to uniform moment loading,* $F_y = 60$ *ksi).*

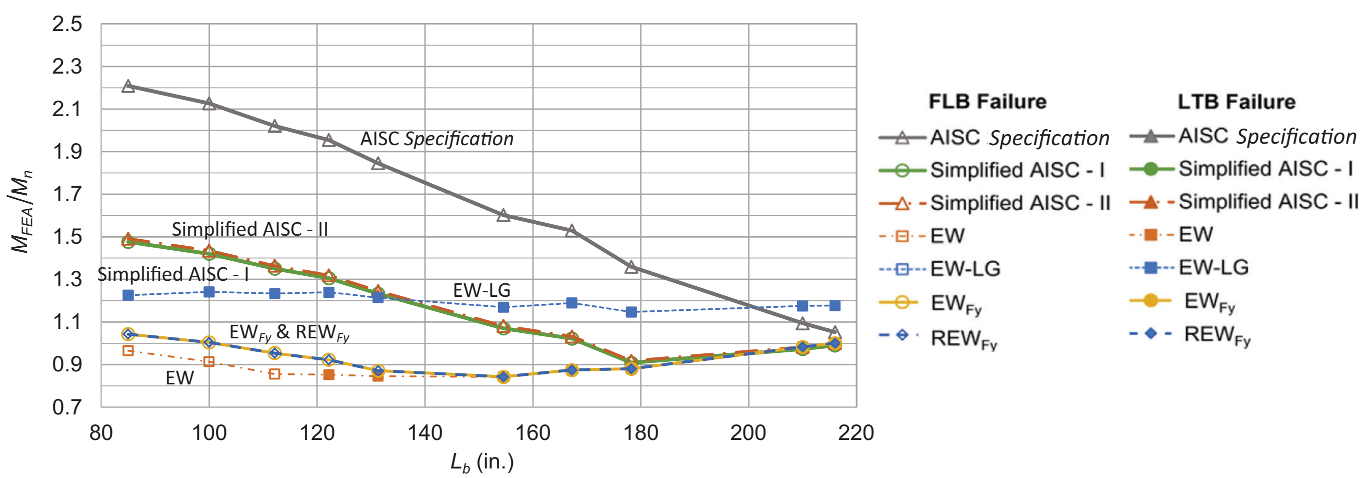

Fig. 11. Comparison of M_{FEA}/M_n *for case 2 members (slender-flange–slender-web members subjected to uniform moment loading,* $F_y = 100$ *ksi).*

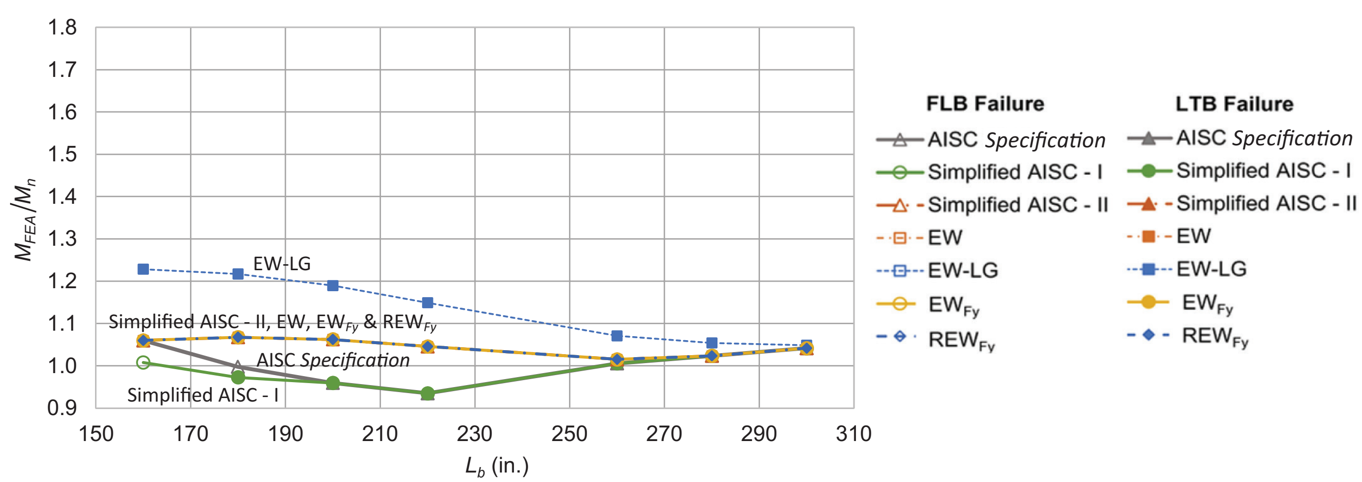

Fig. 12. Comparison of M_{FEA}/M_n *for case 3 members (slender-flange–compact-web members subjected to uniform moment loading,* $F_y = 60$ *ksi).*

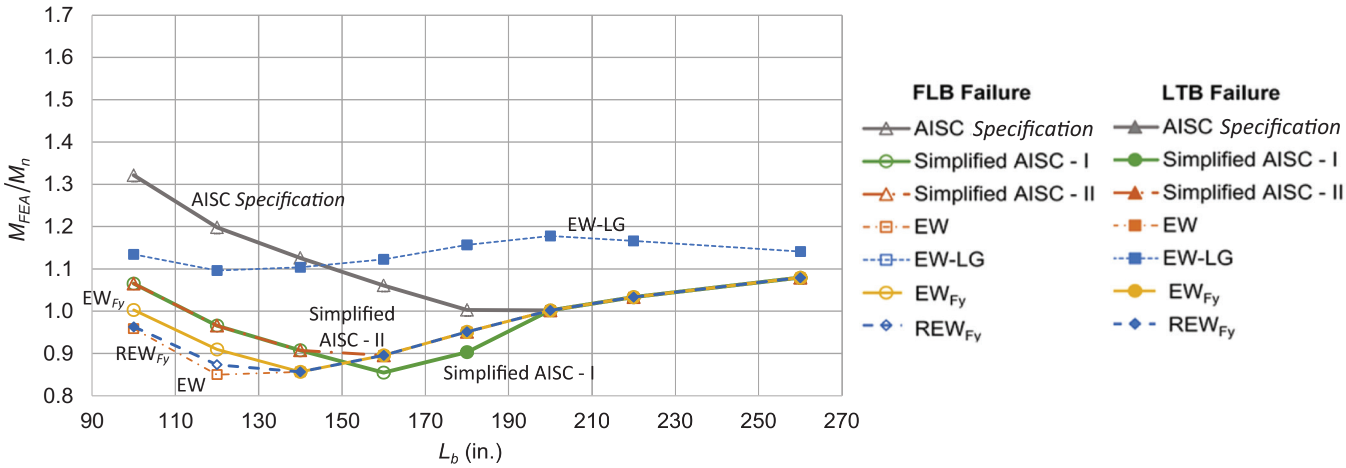

Fig. 13. Comparison of M_{FEA}/M_n *for case 4 members (slender-flange–compact-web members subjected to uniform moment loading,* $F_y = 100$ *ksi).*

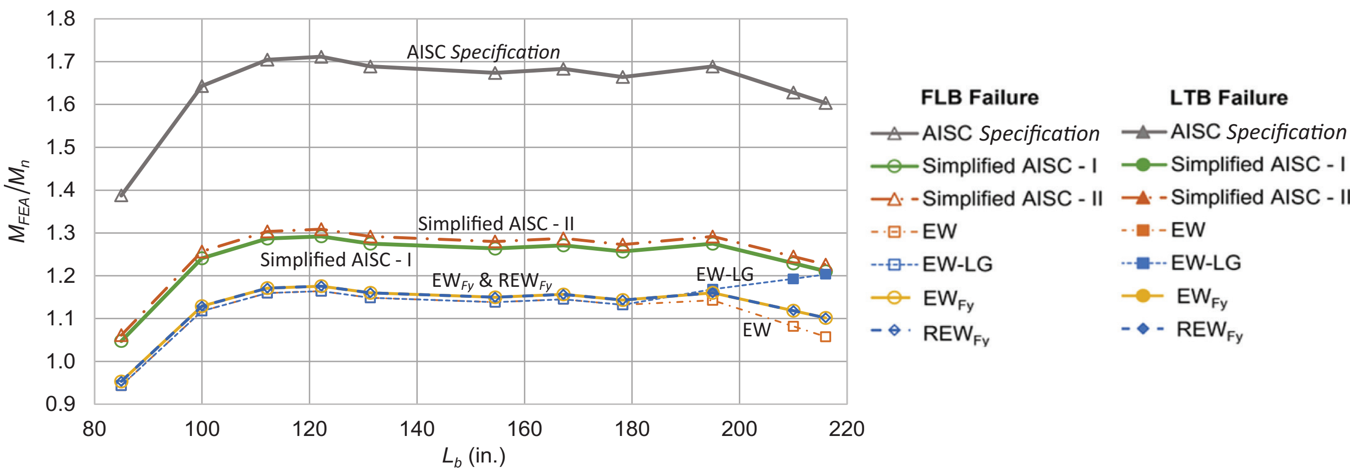

Fig. 14. Comparison of M_{FEA}/M_n *for case 5 members (slender-flange–slender-web members subjected to a linearly varying moment,* $F_y = 60$ *ksi).*

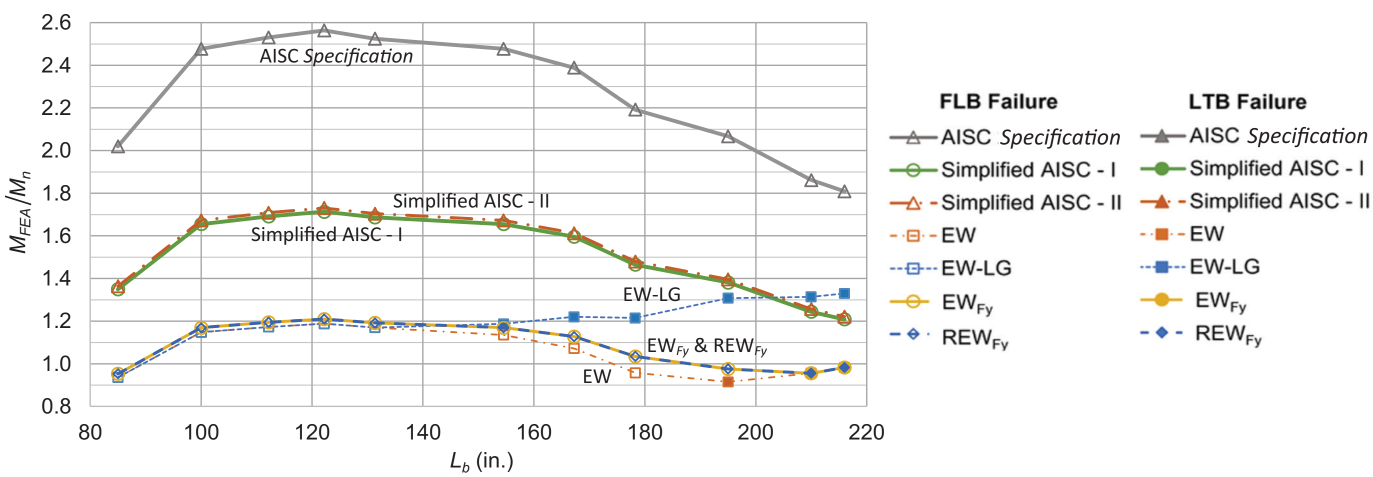

Fig. 15. Comparison of M_{FEA}/M_n *for case 6 members (slender-flange–slender-web sections under a linearly varying moment,* $F_y = 100$ *ksi).*

Table 3. Statistics for Local–Global Buckling Interaction Test Cases							
Category	Statistics	AISC *Specification*	Simplified AISC-I	Simplified AISC-II	EW	EW-LG	EW_{Fy} and REW_{Fy}
All tests	Maximum	2.56	1.71	1.73	1.19	1.33	1.21
	Minimum	0.93	0.85	0.90	0.84	0.94	0.84
	Average	1.54	1.17	1.19	1.01	1.17	1.03
	COV	0.31	0.19	0.19	0.10	0.07	0.09
Tests with F_y = 60 ksi	Maximum	1.71	1.29	1.31	1.16	1.28	1.18
	Minimum	0.93	0.91	0.94	0.94	0.94	0.94
	Average	1.35	1.10	1.13	1.04	1.17	1.06
	COV	0.22	0.12	0.11	0.07	0.07	0.07
Tests with F_y = 100 ksi	Maximum	2.56	1.71	1.73	1.19	1.33	1.21
	Minimum	1.00	0.85	0.90	0.84	0.94	0.84
	Average	1.74	1.25	1.26	0.97	1.18	1.00
	COV	0.32	0.22	0.22	0.11	0.06	0.11
Tests with a compact web	Maximum	1.32	1.08	1.08	1.08	1.23	1.08
	Minimum	0.93	0.85	0.90	0.85	1.05	0.86
	Average	1.06	0.98	1.01	1.00	1.14	1.00
	COV	0.09	0.06	0.06	0.08	0.05	0.07
Tests with a slender web	Maximum	2.56	1.71	1.73	1.19	1.33	1.21
	Minimum	0.94	0.91	0.92	0.84	0.94	0.84
	Average	1.71	1.24	1.26	1.01	1.19	1.04
	COV	0.26	0.18	0.18	0.10	0.07	0.10

to a lack of accounting for local–global interaction. The EW_{Fy} and REW_{Fy} methods give slightly larger M_{FEA}/M_n values on average compared to the EW method (mean $M_{FEA}/M_n = 1.00$ for 100-ksi members and mean $M_{FEA}/M_n =$ 1.03 for all the conducted tests). The overall statistics for the EW_{Fy} and REW_{Fy} procedures are the same to the significant digits shown in Table 3 because these methods give the same strength predictions for most of the tests.

For the moment gradient tests (Figures 14 and 15), all but a few of the test members are predicted to fail in FLB by all of the procedures. The AISC *Specification* procedure gives highly conservative predictions for these cases.

For the compact-web test cases (Figures 12 and 13), the Simplified AISC-II method gives the "best" predictions of all the methods (mean $M_{FEA}/M_n = 1.01$ with a small COV of 0.06, a minimum $M_{FEA}/M_n = 0.90$, and a maximum $M_{FEA}/M_n = 1.08$). The Simplified AISC-II method also performs reasonably well for the test cases with $F_y = 60$ ksi, giving a mean $M_{FEA}/M_n = 1.13$, a COV of 0.11, a minimum M_{FEA}/M_n of 0.94, and a maximum M_{FEA}/M_n of 1.31. However, this method tends to give more conservative predictions and larger dispersion (mean $M_{FEA}/M_n = 1.26$ and COV = 0.22) for the 100-ksi members.

Figure 16 shows an example of significant compression flange local buckling deformations at the peak load for the UM-Lb154-SF-SW-100 test member. The magnified deformed shape (scale factor = 5.0) is plotted showing the von Mises stress contours on the top surface of the flanges.

Comparison with Experimental Data

Figure 17 summarizes the predictions of the strengths from uniform bending experimental tests in which the flexural resistance is governed by flange local buckling based on the AISC *Specification* calculations. The Lew and Toprac (1968) and Carskaddan (1968) tests had flange yield strengths exceeding 100 ksi, whereas the test by Basler et al. (1960) had a compression flange yield strength of only 35.4 ksi. The tests by Holtz and Kulak (1973) had a compression flange yield strength of 46.8 ksi, while the tests by Holtz and Kulak (1975) had a compression flange yield strength of only 34.7 ksi. Johnson's (1985) tests had F_{yc} between 53.7 ksi and 63.4 ksi. All of these specimens were doubly symmetric except for the test by Basler et al., in which the compression flange was larger than the tension flange.

One of the tests from Johnson (1985) and two of the tests from Holtz and Kulak (1973) had compact flanges. As such, the $\lambda_{fc}/\lambda_{pf}$ values for these tests are less than 1.0 in Figure 17, and the flange local buckling resistance corresponds to the flexural strength plateau for these specimens. These tests are included since they were a part of a series of tests that were focused on evaluating flange local buckling resistance.

The specimens tested by Johnson (1985), Basler et al. (1960), and Lew and Toprac (1968) with $\lambda_{fc}/\lambda_{pf} > 1.75$ are classified as slender-flange members per the AISC *Specification*. It is evident that the AISC *Specification* gives conservative strength estimates for these members. This behavior is identified also by the FEA studies discussed previously. This conservatism is mitigated by the other approaches.

The predictions by EW-LG procedure are governed by the LTB resistance (based on effective section properties) for a number of the tests, resulting in slightly larger M_{test}/M_n values in Figure 17(f) compared to those obtained using the other effective width based approaches. While the EW-LG approach tends to gives some of the most conservative predictions for the tests with intermediate flange slenderness values, it performs well in bringing the M_{test}/M_n values close to 1.0 for several of the tests with larger flange slenderness values. The other effective width-based procedures perform well in bringing the mean of M_{test}/M_n closer to 1.0, but they give M_{test}/M_n values significantly less than 1.0 for a number of the tests with larger λ_{fc} values. This is particularly notable for two of the tests with larger $\lambda_{fc}/\lambda_{pf}$ values conducted by Lew and Toprac (1968), which have improved predictions using the EW-LG method; for the single test conducted by Basler et al. (1960), which has relatively small yield strengths and is governed by FLB in all cases; and for several of the tests conducted by Johnson (1985) that had noncompact and compact webs, where the adjustments increasing the corresponding calculated strengths in the REW_{Fy} method result in an over-prediction of the test results ($M_{test}/M_n < 1.0$).

Compared to the more elaborate flange effective width-based approaches discussed in this paper, it is evident that the Simplified AISC approach, which modifies the AISC *Specification* FLB calculations by increasing the ordinate of the second anchor point of the linear equation for noncompact flanges, and extending the use of this equation into the slender-flange range, performs well in predicting accurate to conservative strengths for all the test members.

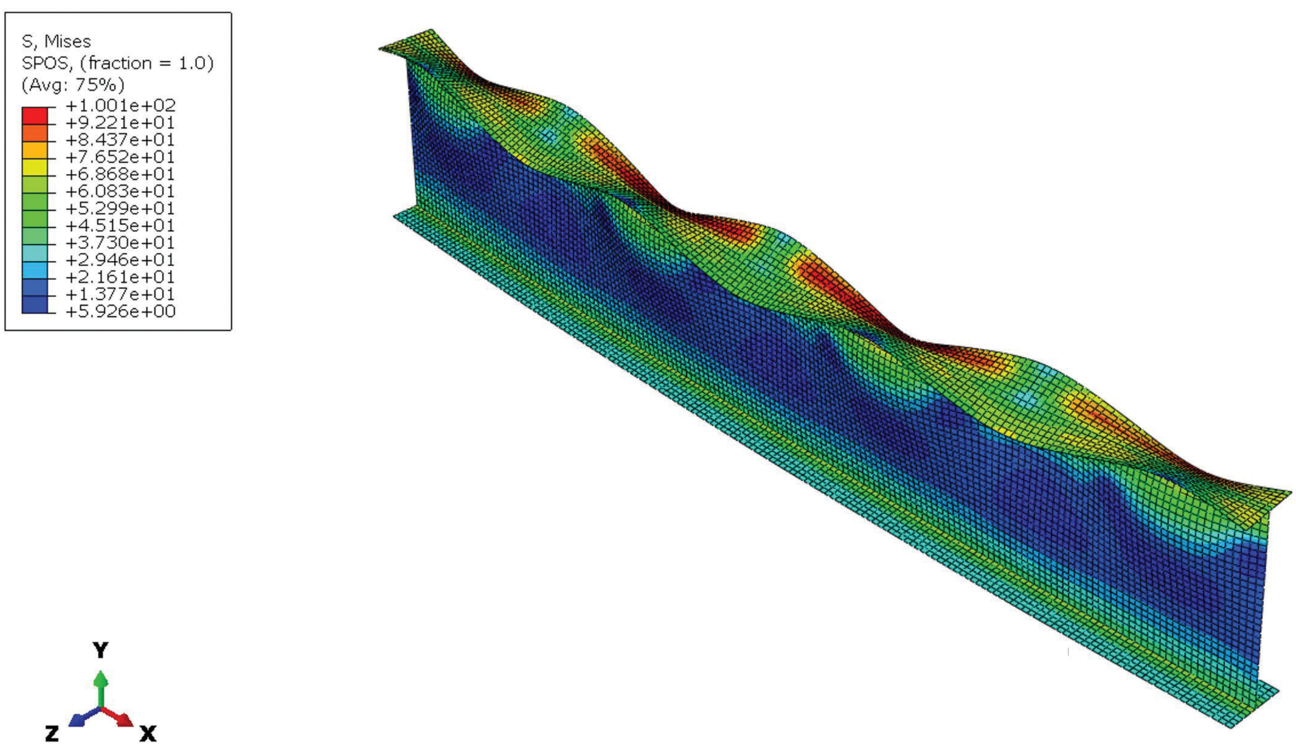

Fig. 16. Deformed shape of UM-Lb154-SF-SW-100 test member at peak load plotted showing the von Mises stress contours at the top surface of the flanges (displacement scale factor = 5.0).

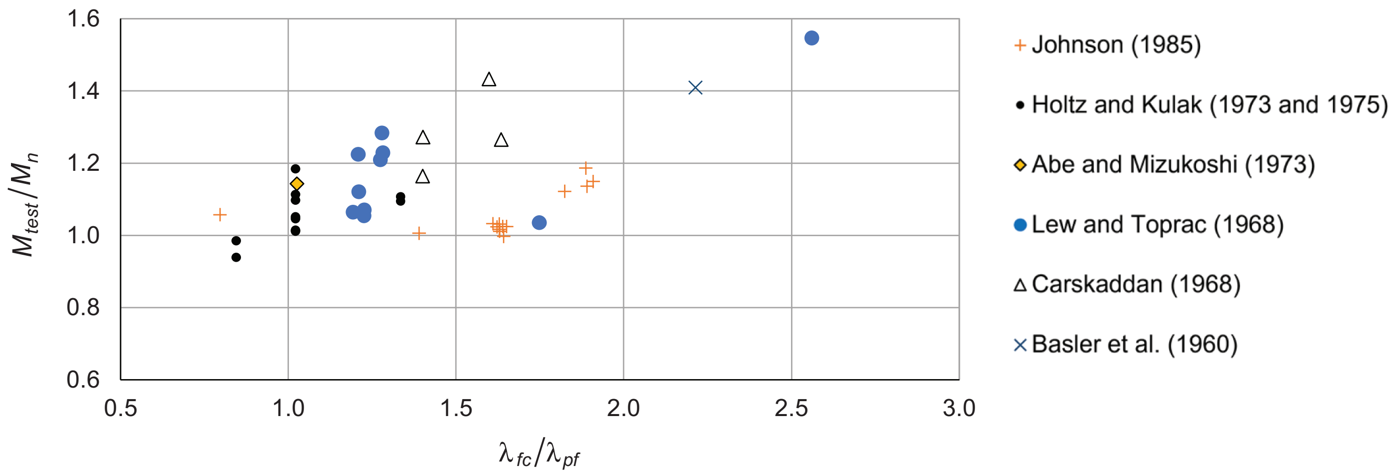

(a) AISC Specification

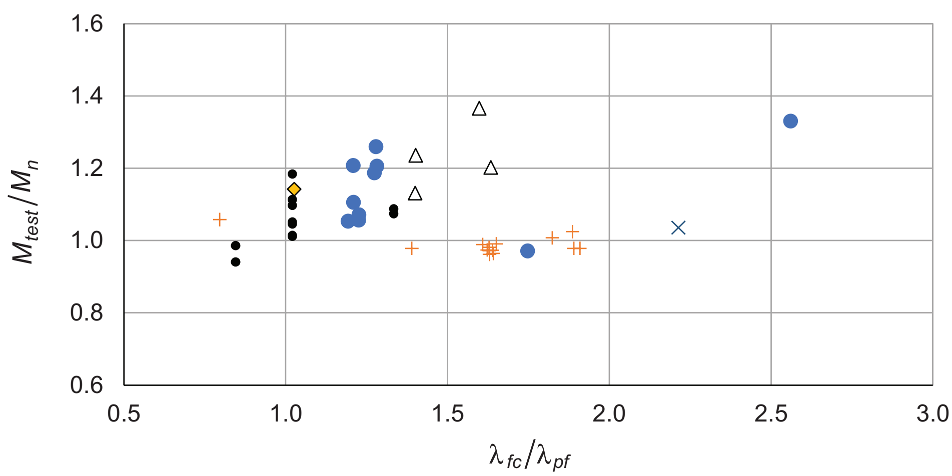

(b) Simplified AISC

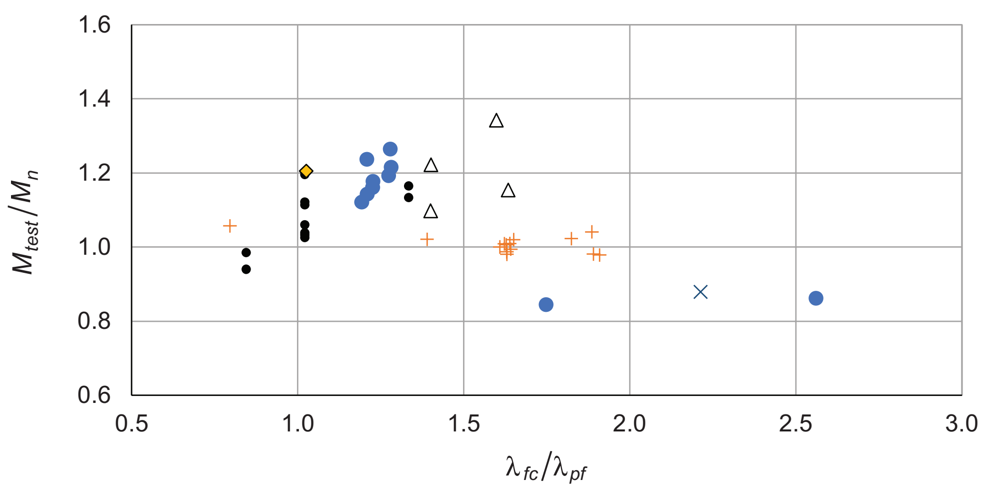

(c) EW

Fig. 17 (a,b,c). Comparison of M_{test}/M_n *for experimental data versus* λ_f/λ_{pf} *for all methodologies studied, uniform bending tests.*

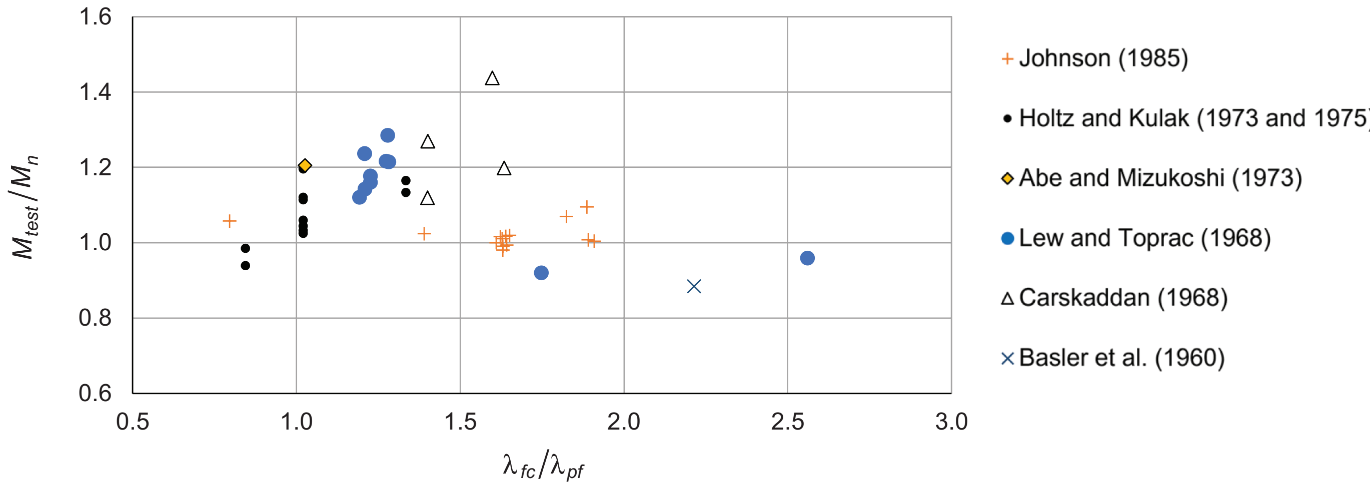

(d) EW_{FY}

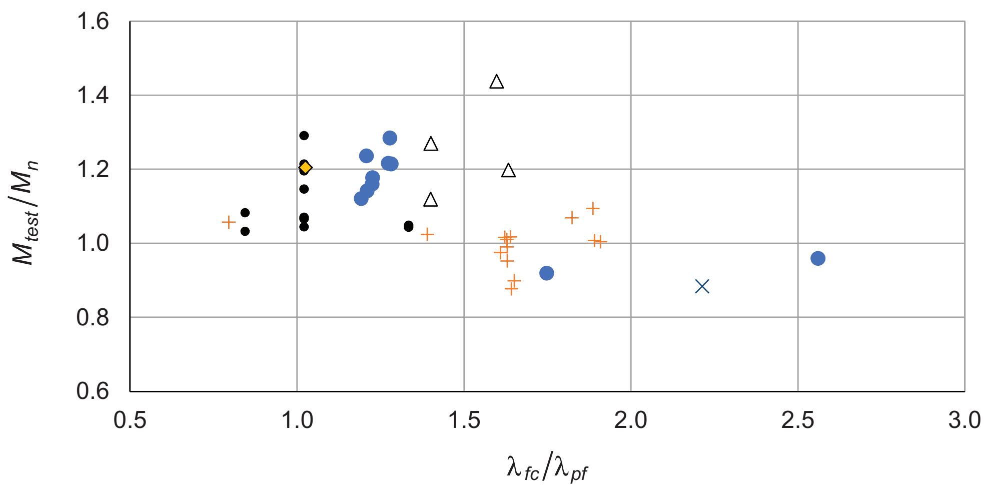

(e) REW_{FY}

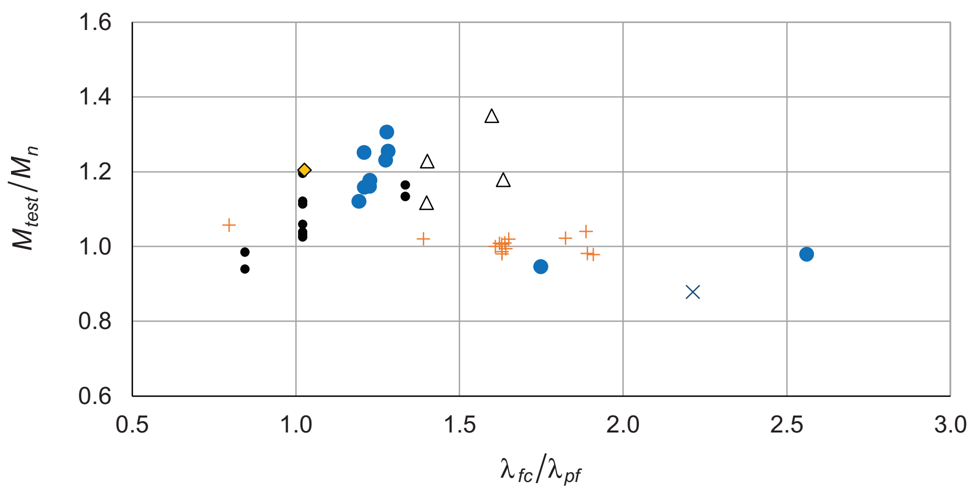

(f) EW-LG

Fig. 17 (d,e,f). Comparison of M_{test}/M_n for experimental data versus λ_f/λ_{pf} for all methodologies studied, uniform bending tests.

Figure 18 summarizes the AISC *Specification* and Simplified AISC calculations for a subset of moment gradient tests cataloged previously by White and Kim (2008), as well as a subset of the tests conducted by Righman (2005), Xiong et al. (2016), and Wang et al. (2021), in which the calculated AISC *Specification* flexural strengths are all governed by FLB. In all of these experimental tests, the flanges classify as noncompact according to the AISC *Specification* and the Simplified AISC provisions. The range of $\lambda_{fc}/\lambda_{pf}$ extends only from 1.01 to 1.60 for the data in Figure 18. None of the FLB strength calculations are influenced by moment gradient. Because the wavelength of the flange local buckles is typically small relative to the variation in the moment along the member length, the impact of moment gradient on the FLB resistance is commonly taken to be negligible. Only the calculated LTB resistances are affected. However, as discussed in Deshpande et al. (2021), the web shear associated with moment gradient, $V = dM/dx$, can influence the web distortion. This in turn may have some impact on the physical FLB resistances. In addition, two of the tests by Schilling (1985), all of the tests by Righman (2005), and one of the tests by Wang et al. (2021) involve singly symmetric I-section members with a smaller flange in compression. The larger depth of the web in compression, combined with the web shear due to the moment gradient, may lead to some challenges in the accurate prediction of the flexural strengths. One practical scenario where the compression flange can be smaller than the tension flange is in composite bridge or building girders, when they are in their noncomposite condition during construction.

All of the tests from Wang et al. (2021), Lew and Toprac (1968), Fahnestock and Sause (1998), and Salem and Sause (2004) considered in Figure 18 entail girders with a measured $F_{yc} > 100$ ksi. The tests by Xiong et al. (2016) focused

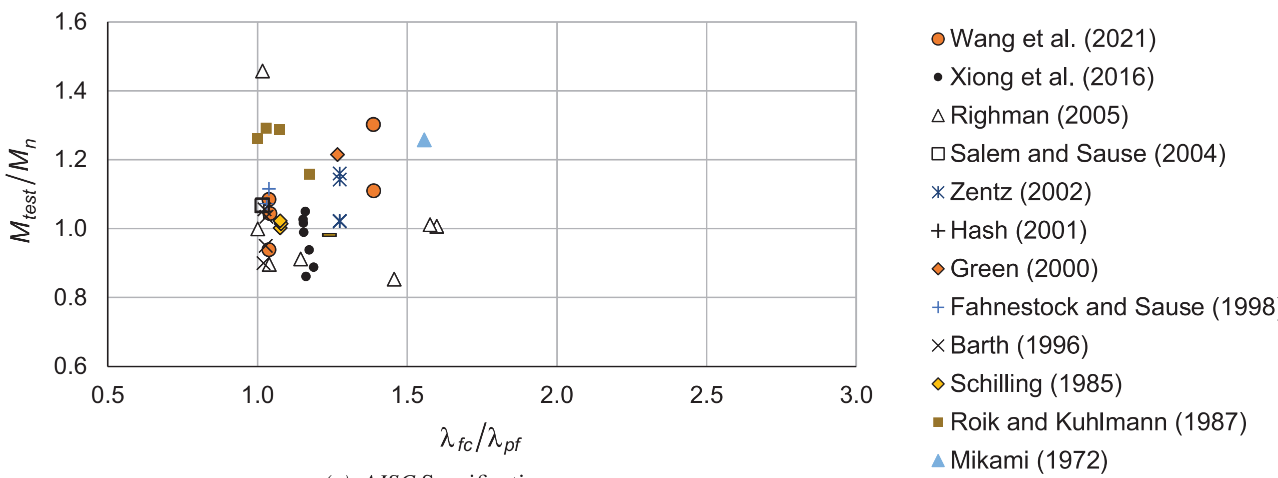

(a) *AISC* Specification

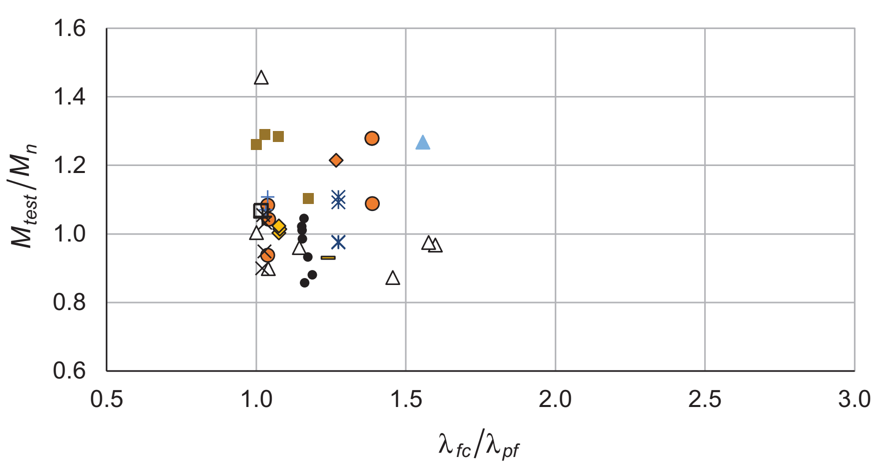

(b) *Simplified AISC*

Fig. 18. Comparison of M_{test}/M_n *for experimental data versus* λ_f/λ_{pf} *for the AISC* Specification *and the Simplified AISC methods, moment gradient tests.*

on I-section members with $F_{yc} = 76.1$ ksi, the test by Green (2000) had $F_{yc} = 86.8$, three of Righman's tests had F_{yc} of 88.2 ksi or larger, and all the tests by Zentz (2001) had $F_{yc} = 91.0$ ksi. Therefore, these tests involve a range of high-strength steels.

One can observe that the predictions from the AISC *Specification* and the Simplified AISC procedures are practically the same for the tests in Figure 18. The mean and COV from the AISC *Specification* calculations is 1.07 and 0.13, respectively, versus 1.06 and 0.13 from the Simplified AISC provisions. It should be noted however that while the predictions from these two procedures are nearly identical for these experimental tests, comprised of members with noncompact flanges, the Simplified AISC procedure would tend to mitigate the conservatism of the AISC *Specification* predictions for slender-flange members. Further experimental testing would be appropriate to provide additional verification of the flange local buckling resistance of I-section members having these characteristics.

Three of the smaller professional bias factors, M_{test}/M_n, from the tests conducted by Xiong et al. (2016) correspond to cases in which the physical member clearly failed by LTB rather than FLB. These tests correspond to LTB slenderness values at which the calculated strengths, scaled by C_b, are truncated by the plateau resistance. Several of the smaller M_{test}/M_n values from Righman (2005) have I_{yc}/I_y values close to or violating the limit of 0.23 in Figure 3, combined with relatively large h/t_w values between 84 and 94 (h_c/t_w = between 95 and 107), relatively large LTB slenderness values, and moment gradient loading. However, one of the Righman (2005) tests that had an I_{yc}/I_y less than 0.23 combined with a web with $h/t_w = 33$ and $h_c/t_w = 41$, as well as relatively small LTB slenderness, exhibited the largest M_{test}/M_n shown in Figure 18 ($M_{test}/M_n = 1.46$). Clearly, there are many attributes of the moment gradient tests that can significantly influence the flexural resistances other than the direct evaluation of FLB. However, the scatter band of the M_{test}/M_n calculations from the AISC *Specification* and the Simplified AISC calculations is comparable to that of the LTB results considered in reliability assessments pertaining to the AISC *Specification* (White and Jung, 2008; White and Kim, 2008; Subramanian et al. 2018; Slein et al., 2021). The test results considered in Figures 17 and 18 are evaluated in more detail in Slein et al. (2021).

CONCLUSIONS

Strength predictions from parametric FEA studies as well as measured strengths collected from previous experimental tests on I-section members failing by FLB show that the AISC *Specification* gives highly conservative results for flexural members having a slender compression flange. The methodologies proposed in this paper successfully mitigate this conservatism by considering the post-buckling strength of slender flanges; however, there are important considerations regarding the efficacy of their use considering their predictions relative to the FEA and experimental test results. These considerations may be summarized as follows:

1. The EW-LG procedure, accounting for slender flange post-buckling strength as well as local–global interaction, gives accurate to conservative predictions in most cases for members with highly slender flanges having 60-ksi and 100-ksi yield strengths. However, comparison with reported experimental strengths shows that it tends to underpredict the strengths for members with intermediate flange slenderness values.
2. The EW, EW_{Fy}, and REW_{Fy} procedures provide adequate predictions for 60-ksi members in the FEA simulation studies, mitigating the conservatism attached with AISC *Specification* predictions for slender-flange members. However, the FEA simulation results show that the predictions for 100-ksi members with slender flanges tend to be slightly unconservative for intermediate unbraced lengths most susceptible to local–global interaction. In addition, several experimental tests of members with yield strengths exceeding 100 ksi show this trend. Although the REW_{Fy} method gave improved predictions in the FEA simulation studies for 60-ksi members, it overpredicts the strengths in a number of experimental tests having compact or noncompact webs.
3. The Simplified AISC procedure provides a straightforward adjustment to the AISC *Specification* calculations for FLB, without requiring the use of flange effective width calculations to account for the post-buckling strength of slender flanges or (in the case of the EW-LG procedure) local–global buckling interactions. This procedure is shown to produce accurate to conservative strength predictions for both the 60-ksi and 10-ksi FEA test simulation cases as well as for experimental tests documented in the literature. The best predictions for this method are obtained with the Simplified AISC-II procedure, which combines the recommended FLB calculations with the use of the LTB strength curve and noncompact web limit parameters recommended by Subramanian et al. (2018) and Subramanian and White (2017b and 2017d).

REFERENCES

Abe, H., and Mizukoshi, N. (1973), "Buckling Tests on Plate Girders under Bending," *Annual Meeting of the Japanese Society of Civil Engineers*, Japan Society of Civil Engineers, Tokyo.

AISC (2016), *Specification for Structural Steel Buildings*, ANSI/AISC 360-16, American Institute of Steel Construction, Chicago, Ill.

ASCE (1971), *Plastic Design in Steel: A Guide and Commentary*, American Society of Civil Engineers, New York, N.Y.

AWS (2020), *Structural Welding Code–Steel*, AWS D1.1:D1.1, American Welding Society, Miami, Fla.

Barth, K.E. (1996), "Moment-Rotation Characteristics for Inelastic Design of Steel Bridge Beams and Girders," Doctoral Dissertation, Department of Civil Engineering, Purdue University, West Lafayette, Ind.

Basler, K., Yen, B., Mueller, J., and Thurlimann, B. (1960), "Web Buckling Tests on Welded Plate Girders," WRC Bulletin No. 64, Welding Research Council, New York, N.Y.

Carskaddan, P. (1968), "The Bending Behavior of Slender-web Girders with A514 Steel Flanges," U.S. Steel Corporation, Applied Research, Report (57.019-904)(5) (AS-EA-23-ps).

CEN (2006), *Eurocode 3: Design of Steel Structures*, 1993-1-5, Comite Européen de Normalisation, Brussels, Belgium.

Cherry, S. (1960), "The Stability of Beams with Buckled Compression Flanges," *Structural Engineering*, Vol. 38, pp. 277–285.

Deshpande, A.M., Kamath, A.M., Slein, R., Sherman, R.J., and White, D.W. (2021), "Built-Up I-Section Member Flexural Resistance: Inelastic C_b Effects from Web Shear Post-Buckling and Early Tension Yielding," SEMM Research Report 21-02, School of Civil and Environmental Engineering, Georgia Institute of Technology, Atlanta, Ga.

Fahnestock, L. and Sause, R. (1998), "Flexural Strength and Ductility of HPS-100W Steel I-Girders," ATLSS Report No. 98-05, Lehigh University, Bethlehem, Pa.

Gerard, L. (2020), "Contribution to the Design of Steel I and H-Sections Members by Means of the Overall Interaction Concept," Doctoral Dissertation, Civil and Water Engineering Department, Laval University, Quebec, Canada.

Green, P.S. (2000), "The Inelastic Behavior of Flexural Members Fabricated from High Performance Steel," Doctoral Dissertation, Department of Civil Engineering, Lehigh University, Bethlehem, Pa.

Hash, J.B. (2001), "Shear Capacity of Hybrid Steel Girders," Master's Thesis, Department of Civil Engineering, University of Nebraska, Neb.

Holtz, N. and Kulak, G. (1973), "Web Slenderness Limits for Compact Beams," Structural Engineering Report No. 43, University of Alberta, Alberta, Canada.

Holtz, N. and Kulak, G. (1975), "Web Slenderness Limits for Noncompact Beams," Structural Engineering Report No. 51, (p. 21). University of Alberta, Alberta, Canada.

Johnson, D. (1985), "An Investigation into the Interaction of Flanges and Webs in Wide Flange Shapes," *Annual Technical Session*, Structural Stability Research Council, pp. 395–405.

Kim, Y.D. (2010), "Behavior and Design of Metal Building Frames Using General Prismatic and Web-Tapered Steel I-Section Members," Doctoral Dissertation, Georgia Institute of Technology, Atlanta, Ga.

Latif, W. (2020), "Flange Local Buckling Resistance and Local-Global Buckling Interaction in Slender-Flange Welded I-Section Beams," MS Thesis, Georgia Institute of Technology, Atlanta, Ga.

Lew, H. and Toprac, A. (1968), "The Static Strength of Hybrid Plate Girders," S.F.R.L. Technical Report P550-11, Structures Fatigue Research Laboratory, Department of Civil Engineering, University of Texas, Austin, Texas.

MBMA (2012), *Metal Building Systems Manual*, Metal Building Manufacturer's Association, Cleveland, Ohio.

Mikami, I. (1972), "Study on Buckling of Thin Walled Girders under Bending," Doctoral Dissertation, Department of Civil Engineering, Nagoya University, Japan (in Japanese).

Peköz, T. (1986), "Development of a Unified Approach to the Design of Cold-Formed Steel Members," Report SG-86-4, American Iron and Steel Institute, Washington, D.C.

Righman, J. (2005), "Rotation Compatibility Approach to Moment Redistribution for Design and Rating of Steel I-Girders," Doctoral Dissertation, School of Civil Engineering, West Virginia University, Morgantown, W.V.

Roik, K. and Kuhlmann, U. (1987), "Rechnerische Ermittlung der Rotationkapazitat biegebeanspruchter I-Profile," *Stahlbau*, Vol. 11, pp. 321–327.

Salem, E.S. and Sause, R. (2004), "Flexural Strength and Ductility of Highway Bridge I-Girders Fabricated from HPS-100W Steel," ATLSS Report No. 04-12.

Schafer, B., Fraser, T., Goel, S., McManus, P., Sherman, D., Sabol, T., Uang, C.-M., Varma, A., and Leu, B. (2020), "Task Group Report on Local Buckling (Width-to-Thickness) Limits," American Institute of Steel Construction, Chicago, Ill.

Schilling, C.G. (1985), "Moment-Rotation Tests of Steel Bridge Girders," Project 188, Autostress Design of Highway Bridges, American Iron and Steel Institute, Washington, D.C.

Seif, M. (2010), "Cross-Section Stability of Structural Steel," Doctoral Dissertation, John Hopkins University, Baltimore, Md.

Seif, M. and Schafer, B. (2010), “Local Buckling of Structural Steel Shapes,” *Journal of Constructional Steel Research*, Vol. 66, pp. 1,232–1,247.

Simulia (2013), *ABAQUS/Standard Version 6.13-1*, Simulia, Inc., Providence, R.I.

Slein, R., Phillips, M.L., Sherman, R.J., and White, D.W. (2021), “Assessment of Built-Up I-Section Member Flexural Resistances from Experimental Test Data,” SEMM Research Report 21-09, School of Civil and Environmental Engineering, Georgia Institute of Technology, Atlanta, Ga.

Subramanian, L. (2015), “Flexural Resistance of Longitudinally Stiffened Plate,” Doctoral Dissertation, Georgia Institute of Technology, Atlanta, Ga.

Subramanian, L.P. and White, D.W. (2017a), “Resolving the Disconnects between Lateral Torsional Buckling Experimental Tests, Test Simulations and Design Strength Equations,” *Journal of Constructional Steel Research*, Vol. 128, pp. 321–334.

Subramanian, L. and White, D.W. (2017b), “Reassessment of the Lateral Torsional Buckling Resistance of I-Section Members: Uniform-Moment Studies,” *Journal of Structural Engineering*, ASCE, Vol. 143, No. 3, DOI: 10.1061/(ASCE)ST.1943-541X.0001686.

Subramanian, L. and White, D.W. (2017c), “Reassessment of the Lateral Torsional Buckling Resistance of Rolled I-Section Members: Moment Gradient Tests,” *Journal of Structural Engineering*, ASCE, Vol. 143, No. 4, DOI: 10.1061/(ASCE)ST.1943-541X.0001687.

Subramanian, L. and White, D.W. (2017d), “Improved Noncompact Web-Slenderness Limit for Steel I-Girders,” *Journal of Structural Engineerin*g, Vol. 143, No. 4, DOI: 10.1061/(ASCE)ST.1943-541X.0001722.

Subramanian, L., Jeong, W.Y., Yellepeddi, R., and White, D.W. (2018), “Assessment of I-Section Member LTB Resistances Considering Experimental Test Data and Practical Inelastic Buckling Design Calculations,” *Engineering Journal*, AISC, Vol. 55, No. 1, pp. 15–44.

Toğay, O. (2018), “Advanced Design Evaluation of Planar Steel Frames Composed of General Nonprismatic I-Section Members,” Doctoral Dissertation, Georgia Institute of Technology, Atlanta, Ga.

Toğay, O. and White, D.W. (2018), “Toward the Recognition of Unaccounted for Flange Local Buckling and Tension Flange Yielding Resistances in the ANSI/AISC 360 *Specification*,” *Proceedings of the Annual Stability Conference Structural Stability Research Council*.

Wang, K., Xiao, M., Chung, K.-F., and Nethercot, D.A. (2021), “Lateral Torsional Buckling of Partially Restrained Beams of High Strength S690 Welded I-Sections,” *Journal of Constructional Steel Research*, Vol. 184, DOI: 10.1016/j.jcsr.2021.106777.

White, D.W., Jeong, W., and Slein, R. (2021), *Frame Design Using Nonprismatic Members*, 2nd Ed., Design Guide 25, AISC, Chicago, Ill.

White, D.W. and Jung, S. (2008), “Unified Flexural Resistance Equations for Stability Design of Steel I-Section Members—Uniform Bending Tests,” *Journal of Structural Engineering*, Vol. 134, No. 9, pp. 1,450–1,470.

White, D.W. and Kim, Y. (2008), “Unified Flexural Resistance Equations for Stability Design of Steel I-Section Members—Moment Gradient Tests,” *Journal of Structural Engineering*, Vol. 134, No. 9, pp. 1,471–1,486.

Winter, G. (1970), *Light Gage Cold-Formed Steel Design Manual: Commentary of the 1968 Edition*, American Iron and Steel Institute, Washington, D.C.

Xiong, G., Kang, S.B., Yang, B., Wang, S., Bai, J., Nie, S., Hu, Y., and Dai, G. (2016), “Experimental and Numerical Studies on Lateral Torsional Buckling of Welded Q460GJ Structural Steel Beams,” *Engineering Structures*, Vol. 126, DOI: 10.1016/j.engstruct.2016.07.050.

Zentz, A. (2002), “Experimental Moment-Shear Interaction and TFA Behavior in Hybrid Plate Girders,” MS Thesis, University of Missouri, Columbia, Mo.